J|A|C|S ARTICLES

Published on Web 02/24/2009

A Combined Theoretical and Experimental Study on the Role of Spin States in the Chemistry of $Fe(CO)_5$ Photoproducts

Maria Besora,[†] José-Luis Carreón-Macedo,[†] Alexander J. Cowan,[‡] Michael W. George,[*,‡] Jeremy N. Harvey,[*,†] Peter Portius,[‡] Kate L. Ronayne,[§] Xue-Zhong Sun,[§] and Michael Towrie[§]

School of Chemistry, University of Nottingham, University Park Nottingham, Nottingham, NG7 2RD, U.K., Centre for Computational Chemistry and School of Chemistry, University of Bristol, Cantock's Close, Bristol, BS8 1TS, U.K., and STFC Rutherford Appleton Laboratory, Chilton, Didcot, Oxfordshire, OX11 QX, U.K.

Received September 9, 2008; E-mail: mike.george@nottingham.ac.uk; jeremy.harvey@bris.ac.uk

Abstract: A combined experimental and theoretical study is presented of several ligand addition reactions of the triplet fragments $^3Fe(CO)_4$ and $^3Fe(CO)_3$ formed upon photolysis of $Fe(CO)_5$. Experimental data are provided for reactions in liquid *n*-heptane and in supercritical Xe (*sc*Xe) and Ar (*sc*Ar). Measurement of the temperature dependence of the rate of decay of $^3Fe(CO)_4$ to produce $^1Fe(CO)_4L$ (L = heptane or Xe) shows that these reactions have significant activation energies of 5.2 ($\pm$0.2) and 7.1 ($\pm$0.5) kcal mol^{-1} respectively. Nonadiabatic transition state theory is used to predict rate constants for ligand addition, based on density functional theory calculations of singlet and triplet potential energy surfaces. On the basis of these results a new mechanism (spin-crossover followed by ligand addition) is proposed for these spin forbidden reactions that gives good agreement with the new experimental results as well as with earlier gas-phase measurements of some addition rate constants. The theoretical work accounts for the different reaction order observed in the gas phase and in some condensed phase experiments. The reaction of $^3Fe(CO)_4$ with H_2 cannot be easily probed in *n*-heptane since conversion to $^1Fe(CO)_4$(heptane) dominates. *sc*Ar doped with H_2 provides a unique environment to monitor this reaction—Ar cannot be added to form $^1Fe(CO)_4Ar$, and H_2 addition is observed instead. Again theory accounts for the reactivity and also explains the difference between the very small activation energy measured for H_2 addition in the gas phase (Wang, W. et al. *J. Am. Chem. Soc.* **1996**, *118*, 8654) and the larger values obtained here for heptane and Xe addition in solution.

Introduction

Combined experimental and computational studies of chemical reactivity can yield remarkable insight into reaction mechanisms and kinetics. This is particularly true for reactions that involve unusual mechanistic features. Addition of ligands to high-spin metal fragments to yield a low-spin complex is an example of such a challenging class of reaction, as these reactions are spin-forbidden. Changes in spin state do not of course prohibit reactions from taking place, but they do lead to a degree of spin-forbiddenness. A number of experimental studies of these reactions have appeared[1] and confirm that such reactions do occur quite readily in many cases, although, in some cases, unexpectedly low reactivity is observed. Additional insight comes from computational studies[2,3] and, in particular, from the location of the lowest-energy points where the potential energy surfaces of different spin cross each other, also called minimum energy crossing points or MECPs.[4] We have recently explored spin-forbidden reactivity in a number of reactions of transition metal compounds and showed that it is possible to understand the reactivity in a qualitative way by locating the relevant minimum energy crossing points.[5] In a more quantitative way, we have applied a form of nonadiabatic transition state theory (NATST)[6] to calculate rate coefficients for spin-forbidden reactions.[3,7,8] So far, however, relatively few quantitative tests of this NATST have been possible, due to the lack of

[†] University of Bristol.
[‡] University of Nottingham.
[§] STFC Rutherford Appleton Laboratory.

(1) (a) Poli, R. *Acc. Chem. Res.* **1997**, *30*, 494–501. (b) Schwarz, H. *Int. J. Mass Spec.* **2004**, *237*, 75–105. (c) Poli, R. *J. Organomet. Chem.* **2004**, *689*, 4291–4304. Detrich, J. L.; Reinaud, O. M.; Rheingold, A. L.; Theopold, K. H. *J. Am. Chem. Soc.* **1995**, *117*, 11745–11748.
(2) Yarkony, D. R. *J. Am. Chem. Soc.* **1992**, *114*, 5406–5411. Ohsaku, M.; Koga, N.; Morokuma, K. *J. Chem. Soc., Perkin Trans. 2* **1993**, 71–74. Cui, Q.; Morokuma, K. *J. Chem. Phys.* **1997**, *107*, 4951–4959. Cui, Q.; Morokuma, K.; Bowman, J. M.; Klippenstein, S. J. *J. Chem. Phys.* **1999**, *110*, 9469–9482. Aschi, M.; Grandinetti, F. *J. Chem. Phys.* **1999**, *111*, 6759–6768.
(3) Harvey, J. N. *Phys. Chem. Chem. Phys.* **2007**, *9*, 331–343.
(4) Koga, N.; Morokuma, K. *Chem. Phys. Lett.* **1985**, *119*, 371–374. Bearpark, M. J.; Robb, M. A.; Schlegel, H. B. *Chem. Phys. Lett.* **1994**, *223*, 269–274. Yarkony, D. R. *J. Phys. Chem.* **1993**, *97*, 4407–4412.
(5) (a) Poli, R.; Harvey, J. N. *Chem. Soc. Rev.* **2003**, *32*, 1–8. (b) Smith, K. M.; Poli, R.; Harvey, J. N. *New J. Chem.* **2000**, *24*, 77–80. (c) Carreon-Macedo, J.-L.; Harvey, J. N. *J. Am. Chem. Soc.* **2004**, *126*, 5789–5797.
(6) Lorquet, J. C.; Leyh-Nihant, B. *J. Phys. Chem.* **1988**, *92*, 4778–4783.
(7) Harvey, J. N.; Aschi, M. *Faraday Discuss.* **2003**, *124*, 129–143.
(8) Harvey, J. N.; Aschi, M. *Phys. Chem. Chem. Phys.* **1999**, *1*, 5555–5563.

suitable experimental data. The reactions of $^3Fe(CO)_4$ studied here provide an ideal opportunity to test the theory.

There have been many experimental and theoretical studies on the reactivity of spin-forbidden reactions particularly using light to generate the reactive intermediates including studies on $CpV(CO)_4$ ($Cp = \eta^5$-C_5H_5),[9] $CpMn(CO)_3$,[10] $Fe(CO)_5$,[11] $Fe(dmpe)_2$,[12] (dmpe = $Me_2PCH_2CH_2PMe_2$), $CpCo(CO)_2$,[13] and (PNP)Co(CO) (PNP = $[^tBu_2PCH_2SiMe_2)_2N]^-$).[14] The photochemistry of $Fe(CO)_5$ has been widely studied, and it has been shown that a key process is the formation of $^1Fe(CO)_4(L)$ from $^3Fe(CO)_4$. The availability of the experimental rates for this spin-forbidden process in a range of conditions means that experimental validation of theoretically predicted rates is now possible. The addition reactions of CO and H_2 with $Fe(CO)_4$ have been studied computationally before,[7,15] and the rate constant for the CO addition was calculated and found to be in reasonable agreement (better than 1 order of magnitude) with the gas-phase experimental value measured at room temperature by Weitz et al.[16,17]

The results of photochemical experiments of $Fe(CO)_5$ have been reviewed and will only be briefly introduced here.[18] Low temperature matrix isolation studies demonstrated that photolysis of $Fe(CO)_5$ generated primarily $^3Fe(CO)_4$[19] and that prolonged irradiation led to the formation of $Fe(CO)_3$.[20] Photolysis of $Fe(CO)_5$ in N_2, CH_4, and Xe matrices at 20 K produced $^3Fe(CO)_4$, and irradiation of $^3Fe(CO)_4$ with near-IR light (*ca.* 2000 cm^{-1}) led to the formation of a new species, $^1Fe(CO)_4(X)$ (X = N_2, CH_4, Xe). Analogous experiments in argon or neon matrices resulted in $^3Fe(CO)_4$ reacting with CO in the matrix forming $Fe(CO)_5$, and there was no evidence for production of $^1Fe(CO)_4(L)$ (L = Ar, Ne).

The photochemistry of $Fe(CO)_5$ has been studied in the gas phase by time-resolved infrared (TRIR) spectroscopy. Weitz et al. investigated the effect of photolysis wavelength and buffer gas pressure on the proportion of $Fe(CO)_4$, $Fe(CO)_3$, and $Fe(CO)_2$ formed.[21,22] Further TRIR kinetic measurements investigated the reactivity of $^3Fe(CO)_4$, $^3Fe(CO)_3$, and $^3Fe(CO)_2$ to CO, H_2, O_2, and other iron carbonyl fragments.[17,22] Ultrafast electron diffraction experiments have been used to investigate the structure of $^1Fe(CO)_4$ in the gas phase,[23] and it has been demonstrated that this is a precursor to the formation of $^3Fe(CO)_4$ in the gas phase.[23,24]

In the condensed phase TRIR spectroscopy has been used on the microsecond time scale to characterize $^1Fe(CO)_4$(cyclohexane)[25] and on the picosecond time scale[10b] to characterize $^3Fe(CO)_4$ in *n*-heptane. Picosecond TRIR experiments in methanol demonstrated that $^1Fe(CO)_4(CH_3OH)$ formation occurs in <42 ps.[26] We have used picosecond and nanosecond TRIR spectroscopy in both conventional and supercritical solvents[27] to monitor the rate of $^3Fe(CO)_4$ decay and $^1Fe(CO)_4$(solvent) formation in *n*-heptane, supercritical Xe (*sc*Xe), and CH_4 (*sc*CH_4).[28] However, experiments in very weakly coordinating solvents, *sc*Ar[28] and *sc*Kr,[29] demonstrated that $^1Fe(CO)_4L$ (L = Ar, Kr) formation was not formed following the decay of $^3Fe(CO)_4$ and this was consistent with the original low temperature matrix isolation experiments by Poliakoff and Turner.[19] TRIR experiments in cyclohexane have shown that $Fe(CO)_3$, which forms following $Fe(CO)_5$ photolysis, is very short-lived (<1 μs), and it has been proposed that the primary reaction with CO to form $Fe(CO)_4$(cyclohexane) is a significant decay pathway.[30] $^3Fe(CO)_3$(hexane) has been sown to be important in alkene isomerization.[31]

The structures of singlet and triplet $Fe(CO)_4$, and their relative energy, have been studied computationally by a number of authors using different methods.[7,15,32−35] In almost all cases, a triplet ground state is obtained. In one of the earliest studies, it was noted that the addition of CO to $^3Fe(CO)_4$ is spin-forbidden and the occurrence of the reaction was rationalized by spin−orbit coupling.[32] Most computational methods give similar geometries for each of the two spin states, with both species best described as adopting distorted truncated trigonal bipyramidal structures, corresponding to removal of an equatorial carbonyl ligand from $Fe(CO)_5$. The singlet state is predicted to be closer to the idealized truncated trigonal bipyramid, with the angle between the two pseudoaxial ligands closer to 180° and

(9) Snee, P. T.; Yang, H.; Kotz, K. T.; Payne, C. K.; Harris, C. B. *J. Phys. Chem. A* **1999**, *103*, 10426–10432.
(10) (a) Yang, H.; Asplund, M. C.; Kotz, K. T.; Wilkens, M. J.; Frei, H.; Harris, C. B. *J. Am. Chem. Soc.* **1998**, *120*, 10154–10165. (b) Snee, P. T.; Payne, C. K.; Kotz, K. T.; Yang, H.; Harris, C. B. *J. Am. Chem. Soc.* **2001**, *123*, 2255–2264.
(11) Poliakoff, M.; Turner, J. J. *Angew. Chem., Int. Ed.* **2001**, *40*, 2809–2812.
(12) Hall, C.; Jones, W. D.; Mawby, R. J.; Osman, R.; Perutz, R. N.; Whittlesey, M. K. *J. Am. Chem. Soc.* **1992**, *114*, 7425–7435. Macgregor, S. A.; Eisenstein, O.; Whittlesey, M. K.; Perutz, R. N. *J. Chem. Soc., Dalton Trans.* **1998**, 291.
(13) Bengali, A. A.; Bergman, R. G.; Moore, C. B. *J. Am. Chem. Soc.* **1995**, *117*, 3879–3880. Siegbahn, P. E. M. *J. Am. Chem. Soc.* **1996**, *118*, 1487–1496.
(14) Rimmer, R. D.; Grills, D. C.; Fan, H.; Ford, P. C.; Caulton, K. G. *J. Am. Chem. Soc.* **2008**, *129*, 15430–15431. Ingleson, M. J.; Pink, M.; Fan, H.; Caulton, K. G. *J. Am. Chem. Soc.* **2008**, *129*, 4262–4276.
(15) Harvey, J. N.; Poli, R. *Dalton Trans.* **2003**, 4100–4106.
(16) Ouderkirk, A. J.; Weitz, E. *J. Chem. Phys.* **1983**, *79*, 1089–1091.
(17) Ryther, R. J.; Weitz, E. *J. Phys. Chem.* **1991**, *95*, 9841–9852.
(18) Leadbeater, N. *Coord. Chem. Rev.* **1999**, *188*, 35–70.
(19) Poliakoff, M.; Turner, J. J. *J. Chem. Soc., Dalton Trans.* **1974**, 2276–2285.
(20) Poliakoff, M. *J. Chem. Soc., Dalton Trans.* **1974**, 210–212.
(21) Ryther, R. J.; Weitz, E. *J. Phys. Chem.* **1992**, *96*, 2561–2567.
(22) Seder, T. A.; Ouderkirk, A. J.; Weitz, E. *J. Chem. Phys.* **1986**, *85*, 1977–1986.
(23) Ihee, H.; Cao, J.; Zewail, A. H. *Angew. Chem., Int. Ed.* **2001**, *40*, 1532–1536.
(24) Trushin, S. A.; Fuss, W.; Kompa, K. L.; Schmid, W. E. *J. Phys. Chem. A* **2000**, *104*, 1997–2006.
(25) Church, S. P.; Grevels, F. W.; Hermann, H.; Kelly, J. M.; Klotzbucher, W. E.; Schaffner, K. *J. Chem. Soc., Chem. Commun* **1985**, 594–596. Grevels, F. W. In *Photoprocesses in Transition Metal Complexes, Biosystems and Other Molecules*; Kochanski, E., Ed.; Kluwer: Amsterdam, 1992.
(26) Snee, P. T.; Payne, C. K.; Mebane, S. D.; Kotz, K. T.; Harris, C. B. *J. Am. Chem. Soc.* **2001**, *123*, 6909–6915.
(27) Kuimova, M. K.; Alsindi, W. Z.; Dyer, J.; Grills, D. C.; Jina, O. S.; Matousek, P.; Parker, A. W.; Portius, P.; Sun, X. Z.; Towrie, M.; Wilson, C.; Yang, J. X.; George, M. W. *Dalton Trans.* **2003**, 3996–4006.
(28) Portius, P.; Yang, J. X.; Sun, X.-Z.; Grills, D. C.; Matousek, P.; Parker, A. W.; Towrie, M.; George, M. W. *J. Am. Chem. Soc.* **2004**, *126*, 10713–10720.
(29) Sun, X.-Z.; Portius, P.; Grills, D. C.; Cowan, A. J.; George, M. W. *Appl. Spectrosc.* **2008**, *62*, 24–29.
(30) Bachler, V.; Grevels, F. W.; Kerpen, K.; Olbrich, G.; Schaffner, K. *Organometallics* **2003**, *22*, 1696–1711.
(31) Glascoe, E. A.; Sawyer, K. R.; Shanoski, J. E.; Harris, C. B. *J. Phys. Chem. C* **2007**, *111*, 8789–8795.
(32) Daniel, C.; Benard, M.; Dedieu, A.; Wiest, R.; Veillard, A. *J. Phys. Chem.* **1984**, *88*, 4805–4811.
(33) Barnes, L. A.; Rosi, M.; Bauschlicher, C. W. *J. Chem. Phys.* **1991**, *94*, 2031–2039. Gonzalez-Blanco, O.; Branchadell, V. *J. Chem. Phys.* **1999**, *110*, 778–783. Heitz, M.-C.; Daniel, C. *J. Am. Chem. Soc.* **1997**, *119*, 8269–8275.
(34) Carreon-Macedo, J. L.; Harvey, J. N. *Phys. Chem. Chem. Phys.* **2006**, *8*, 93–100.
(35) Wang, W.; Weitz, E. *J. Phys. Chem. A* **1997**, *101*, 2358–2363.

that between the pseudoequatorial ligands closer to 120°. The splitting between the two states is not known experimentally, and computational predictions vary considerably. Most *ab initio* correlated methods predict a large splitting of 10 kcal/mol or more, whereas DFT methods give results between 0 and over 20 kcal/mol depending on the exchange functional used. A recent large basis set CCSD(T) study predicted a small splitting of ca. 2 kcal/mol, and support for this small value was also provided based on calculation of the bond energies of weak ligands such as Xe and CH_4.[34] Modified density functionals with 10% and 15% of exact exchange[36] have been shown to reproduce this energy gap better than standard functionals such as BP86 and B3LYP, which respectively under- and overestimate it.[7]

The binding and activation of dihydrogen to organometallic complexes is a fundamental step in many catalytic mechanisms and is of particular interest to the photochemistry of $Fe(CO)_5$, as it has been previously shown that the photolysis of $Fe(CO)_5$ leads to the formation of an active alkene hydrogenation catalyst.[37,38] The UV photolysis of $Fe(CO)_5$, in the presence of H_2, has been shown to lead to the formation of the dihydride complex $Fe(CO)_4H_2$[17,39] and also the nonclassical dihydrogen complex $Fe(CO)_3(H_2)$.[38] $^1Fe(CO)_4H_2$ has been characterized in low temperature matrices,[40] in the gas phase[41,42] and in solution.[39,43] In the gas phase the rate constant for the oxidative addition of dihydrogen to $^3Fe(CO)_4$ was shown to be ~3 orders of magnitude smaller than typical values for the addition of H_2 to coordinatively unsaturated metal centers.[41] In solution there is evidence for the formation of $^1Fe(CO)_4H_2$ following the photolysis of $Fe(CO)_5$ in methylcyclohexane-d_{14} under a pressure of H_2 at 193 K;[39] however the rate of dihydrogen activation was not reported.

In this paper we report a combined TRIR and DFT study to probe the photochemistry of $Fe(CO)_5$. We show how nonadiabatic transition state theory can be used to obtain theoretical reaction rates for the reaction of $^3Fe(CO)_4$ to $^1Fe(CO)_4(L)$ with a very good agreement with the reported experimental results. We have experimentally obtained activation barriers for the spin forbidden reaction of $^3Fe(CO)_4$ to $^1Fe(CO)_4(L)$ (L = *n*-heptane and Xe), and these can be directly compared to those obtained theoretically. We also investigate the photochemistry of $Fe(CO)_5$ in *sc*Ar solution in the presence of hydrogen, to monitor the activation of H_2, and these results are used to inform and guide further theoretical investigations.

Experimental Details

$Fe(CO)_5$ (Aldrich), CO (Air products, premier grade), Xe (BOC, 99.9995%), Ar (BOC, pureshield grade), and H_2 (BOC, premier grade) were used as supplied. *n*-Heptane (HPLC grade, Aldrich) was distilled from CaH_2 under Ar and degassed prior to use. Solutions were prepared with $Fe(CO)_5$ concentrations in the range $10^{-3}-10^{-4}$ M; in all cases the absorbance at the ν(CO) band maxima of $Fe(CO)_5$ and at 266 nm was kept below unity. Experiments in *n*-heptane were carried out using a 1.5 mm path length CaF_2 cell (Harrick corporation) under 2 atm of CO. To prevent sample degradation, resulting from the high repetition rate UV pump laser (1 kHz), solutions were rapidly recirculated around a closed system. Changes in solution temperature were achieved by use of a cell heating jacket, and the solution temperature was monitored by a thermocouple housed within the cell.

Supercritical xenon (*sc*Xe) solutions containing $Fe(CO)_5$ and CO (60 psi) were prepared in a high-pressure cell described previously for conventional spectroscopic monitoring.[44] The cell was used with CaF_2 windows (4 mm path length). Solutions were recirculated through a stainless steel flow system containing a pressure transducer (RDP Electronics) by a high pressure pump (Micropump Corporation). A constant cell temperature was achieved by use of an external cell heating jacket, and the supercritical fluid temperature was monitored by a thermocouple within the IR cell. Supercritical argon (*sc*Ar) solutions were prepared using an analogous version of the recirculating flow apparatus containing a specially designed picosecond supercritical fluid cell with MgF_2 windows, which has recently been described in detail elsewhere.[29]

To minimize changes in solvent density during the variable temperature *n*-heptane studies, large volumes of the recirculating system were immersed in a constant temperature water bath set at the cell temperature. This will not completely negate any changes in the solvent density, but it should be noted that over the temperature range studied at worst only a small change in solvent density (*ca.* 0.3 mol L^{-1}) would be expected which would be expected to have a neglible influence on the effect measured. This was taken to be sufficient to provide a constant *n*-heptane density in the IR cell. FTIR spectra were recorded before and after each TRIR measurement to monitor $Fe(CO)_5$ concentration and the correct operation of the recirculating flow system. The density of the *sc*Xe solution was controlled by further addition of Xe to the system as the cell temperature was increased ensuring a constant density of Xe (13.3 mol L^{-1}) in the IR cell. FTIR spectra were recorded before each TRIR measurement to ensure that the solvent density was consistent throughout the experiments.

Time-resolved infrared (TRIR) studies were performed on the modified PIRATE apparatus at the Rutherford Appleton Laboratory, which has been described in detail elsewhere.[45,46] Briefly, part of the output from a 1 kHz, 800 nm, 150 fs, 1 mJ Ti:Sapphire oscillator/regenerative amplifier (Spectra Physics) was used to pump a white light continuum-seeded β-barium borate (BBO) optical parametric amplifier (OPA). The signal and idler produced by this OPA were difference frequency mixed in a type I $AgGaS_2$ crystal to generate tuneable mid-infrared IR pulses (ca. 150 cm^{-1} fwhm, *ca.* 100 nJ). The probe pulses were imaged onto the input slit of a 0.25 m mid-IR spectrograph (CVI Laser Corp., DKSP240). Changes in IR absorption were obtained by normalizing the outputs from two 64-element HgCdTe IR array detectors (Infrared Associates Inc.) and subtracting the pump on and pump off data pairs. TRIR spectra on the nanosecond time scale were obtained using a nanosecond laser (1 kHz) to photolyze the sample and probe using the femtosecond IR pulses described above.[46] The nanosecond pump laser and the femtosecond IR spectrometer were synchronized electronically.

(36) Reiher, M.; Salomon, O.; Hess, B. A. *Theor. Chem. Acc.* **2001**, *107*, 48–55.
(37) Schroeder, M. A.; Wrighton, M. S. *J. Am. Chem. Soc.* **1976**, *98*, 551–558.
(38) Hayes, D. M.; Weitz, E. *J. Phys. Chem.* **1991**, *95*, 2723–2727.
(39) Krusic, P. J.; Jones, D. J.; Roe, D. C. *Organometallics* **1986**, *5*, 456–460.
(40) Sweany, R. L. *J. Am. Chem. Soc.* **1981**, *103*, 2410–2412. Cooper, A. I.; Poliakoff, M. *Chem. Phys. Lett.* **1993**, *212*, 611–616.
(41) Wang, W.; Narducci, A.; House, P.; Weitz, E. *J. Am. Chem. Soc.* **1996**, *118*, 8654–8657.
(42) McNeill, E. A.; Scholer, F. R. *J. Am. Chem. Soc.* **1977**, *99*, 6243–6249. Cotton, J. D.; Bruce, M. I.; Stone, F. G. A. *J. Chem. Soc. A* **1968**, 2162–2165.
(43) Farmery, K.; Kilner, M. *J. Chem. Soc. A* **1970**, 634–639.
(44) Poliakoff, M.; Howdle, S. M.; Kazarian, S. G. *Angew. Chem., Int. Ed.* **1995**, *34*, 1275–1295.
(45) Towrie, M.; Grills, D. C.; Dyer, J.; Weinstein, J. A.; Matousek, P.; Barton, R.; Bailey, P. D.; Subramaniam, N.; Kwok, W. M.; Ma, C. S.; Phillips, D.; Parker, A. W.; George, M. W. *Appl. Spectrosc.* **2003**, *57*, 367–380.
(46) Towrie, M.; Gabrielsson, A.; Matousek, P.; Parker, A. W.; Rodriguez, A. M. B.; Vlcek, A. *Appl. Spectrosc.* **2005**, *59*, 467–473.

Computational Details. All species have been fully optimized using the Gaussian 03 program package[47] using the B3PW91** form of density functional theory, followed by computation of frequencies at the same level of theory, within the harmonic approximation. The B3PW91** functional refers to the standard B3PW91 functional[48] in which the proportion of exact exchange has been decreased from 20% to 10%. In the DFT calculations, the all-electron triple-ζ basis sets of Ahlrichs et al.[49] were used for all atoms except Xe. These basis sets were extended as previously[7] by including two diffuse *p* functions[50] and an *f* polarization function on Fe, a *d* polarization function on C and O, and a *p* function on H. The Xe atom was described using a relativistic core potential[51] with the associated polarized VTZ basis set.[52] The minimum energy crossing points were located at the same level of theory by using a minimization code developed by Harvey and Aschi.[53] Unless mentioned otherwise, all energies contain a correction for zero-point energy (zpe). All optimized geometries are included as Cartesian coordinates in the Supporting Information. Calibration CCSD(T) energies and details of the calculation of the root-mean-square of the spin orbit coupling computed are presented in the Supporting Information.

Experimental Determination of Activation Energies. TRIR spectroscopy has previously been used to directly monitor the conversion of $^3Fe(CO)_4$ to $^1Fe(CO)_4$(solvent) following the photolysis of $Fe(CO)_5$ in a range of solvents (*sc*Xe, *sc*CH_4, and *n*-heptane).[28] To provide experimental data to validate the theoretical results discussed below and to gain further insight into the formation of these solvent complexes, we have monitored how the rate of decay of $^3Fe(CO)_4$ and formation of $^1Fe(CO)_4$(solvent) (solvent = *sc*Xe and *n*-heptane) varies with temperature at a constant solvent density.

In agreement with a previous study,[28] following photolysis (266 nm) of $Fe(CO)_5$ in *n*-heptane in the presence of CO (30 psi), ν(CO) bands corresponding to $^3Fe(CO)_4$ (1988 and 1967 cm^{-1}) and $^3Fe(CO)_3$(*n*-heptane) (1926 cm^{-1}) are observed. As the $^3Fe(CO)_4$ bands decay, ν(CO) bands for $^1Fe(CO)_4$(*n*-heptane) (2083, 1989, 1973, and 1953 cm^{-1}) are seen to grow in, Figure 1. The rate of this process (k_{obs} = 7.6 ($\pm$0.1) $\times$ 10^7 s^{-1}) can be monitored at 1970 cm^{-1} ($^3Fe(CO)_4$) and 1952 cm^{-1} ($^1Fe(CO)_4$(heptane)), Figure 2.

A similar experiment has been carried out on the photolysis of $Fe(CO)_5$ (266 nm) in *sc*Xe (1440 psi, 299.4 K) in the presence of CO (60 psi). Initially following photolysis, ν(CO) bands, which could be assigned to $^3Fe(CO)_4$ (1993 and 1972 cm^{-1}) and $^3Fe(CO)_3Xe$ (1931 cm^{-1}) by comparison to previous TRIR studies, were observed (figure in Supporting Information).[28] As the ν(CO) bands of $^3Fe(CO)_4$ decayed, bands corresponding to $^1Fe(CO)_4Xe$ were seen to grow in (1990, 1974, 1961 cm^{-1}). The rise and decay of the bands was ratioed to the parent ν(CO) band absorption to account for any back reaction with CO to reform $Fe(CO)_5$.

Increasing the temperature of the solution significantly accelerates the $^3Fe(CO)_4$ to $^1Fe(CO)_4$(solvent) conversion. Figure 3 shows the Arrhenius plots for these systems. The activation energies obtained in *sc*Xe (7.1 ($\pm$0.5) kcal mol^{-1}) and *n*-heptane (5.2 ($\pm$0.2) kcal mol^{-1}) are of a similar magnitude and are in very good agreement with the calculated activation energy for the reaction of $^3Fe(CO)_4$ to form $^1Fe(CO)_4Xe$ reported below (6.3 kcal mol^{-1}). Indeed, measurement of the activation energies was carried out with the deliberate aim of providing more information on the mechanism and a more stringent test of the theoretical predictions. It is interesting to note that the original experiments carried out in low temperature matrices of CH_4 and Xe required IR irradiation with a source of *ca.* 2000 cm^{-1} (*ca.* 5.7 kcal mol^{-1}) which is in very good agreement with the activation energies determined in room temperature solution.[54]

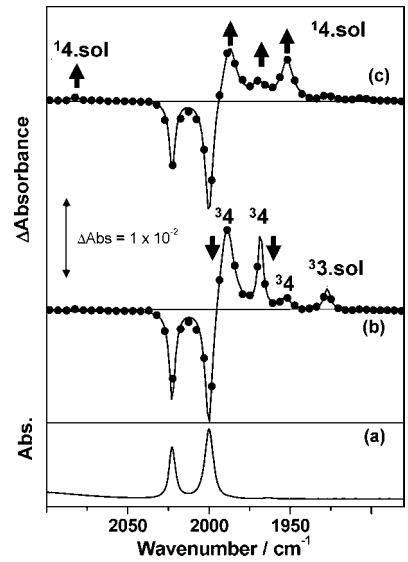

Figure 1. (a) FTIR of $Fe(CO)_5$ in *n*-heptane under CO (20 psi). TRIR difference spectrum of the same solution at 298 K, recorded at (b) 2 ns and (c) 50 ns after photolysis (266 nm). **^{3}4** = $^3Fe(CO)_4$, **^{3}3.sol** = $^3Fe(CO)_3$(*n*-heptane), and **^{1}4.sol** = $^1Fe(CO)_4$(*n*-heptane).

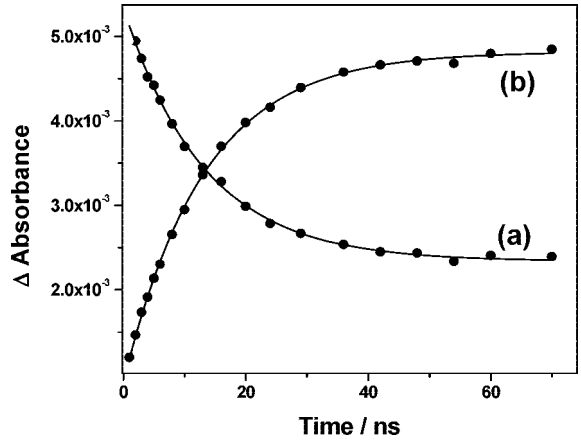

Figure 2. Kinetic trace of (a) the decay of $^3Fe(CO)_4$ (1970 cm^{-1}) and (b) rise of $^1Fe(CO)_4$(*n*-heptane) (1952 cm^{-1}) at 298 K.

Computational Results. Iron tetracarbonyl has a triplet ground state, with the singlet excited state lying 2−3 kcal/mol higher in energy based on accurate CCSD(T) calculations and comparison with experiment.[34] The present B3PW91** level of theory was chosen to survey potential energy surfaces, as, unlike many other functionals, it gives results in reasonable agreement with this, with an energy difference of 3.5 kcal/mol. The two spin states have similar distorted saddle (or truncated trigonal bipyramidal) geometries (Figure 4), and our calculated bond lengths and angles are very close to those reported previously.[7,15,32−35] The singlet adducts $Fe(CO)_4Xe$, $Fe(CO)_5$,[34] and the nonclassical dihydrogen complex, $Fe(CO)_4(H_2)$,[35] have trigonal bipyramidal geometries, again similar to those reported previously, whereas the dihydride[35] $Fe(CO)_4H_2$ has a distorted octahedral structure (Figure 4). The binding energy of Xe is small, whereas CO and H_2 bind significantly more strongly.

(47) Frisch, M. J. et. al. *Gaussian 03*; Gaussian, Inc: Wallingford, CT, 2004.
(48) Becke, A. D. *J. Chem. Phys.* **1993**, *98*, 5648–5652.
(49) Schäfer, A.; Horn, H.; Ahlrichs, R. *J. Chem. Phys.* **1992**, *97*, 2571–2577.
(50) Wachters, A. J. *J. Chem. Phys.* **1970**, *52*, 1033–1036.
(51) Bergner, A.; Dolg, M.; Küchle, W.; Stoll, H.; Preuβ, H. *Mol. Phys.* **1993**, *80*, 1431–1441.
(52) Martin, J. M. L.; Sundermann, A. *J. Chem. Phys.* **2001**, *114*, 3408–3420.
(53) Harvey, J. N.; Aschi, M.; Schwarz, H.; Koch, W. *Theor. Chem. Acc.* **1998**, *99*, 95–99.
(54) Poliakoff, M. *Chem. Soc. Rev.* **1978**, 527–540.

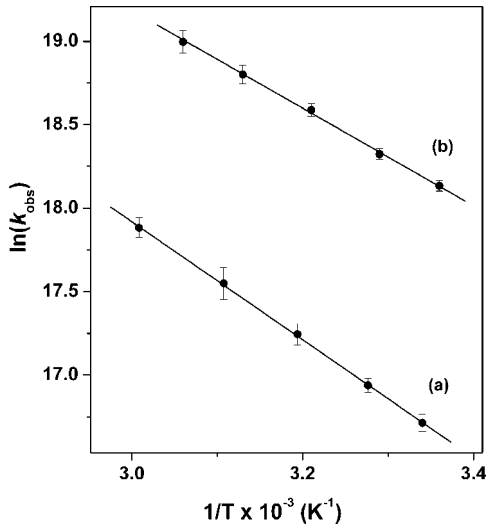

Figure 3. Arrhenius plots of the reaction of $^3Fe(CO)_4$ to $^1Fe(CO)_4$(solvent) (solvent = (a) scXe (13.3 mol L^{-1}) and (b) liquid *n*-heptane).

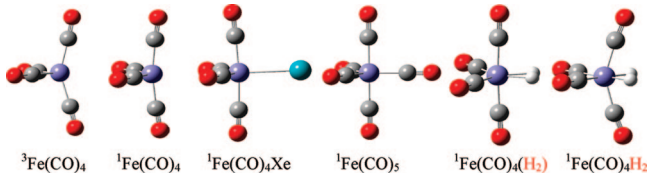

Figure 4. Geometries of the triplet and singlet $Fe(CO)_4$, $^1Fe(CO)_4Xe$, $^1Fe(CO)_5$, $^1Fe(CO)_4(H_2)$, and $^1Fe(CO)_4H_2$.

Scheme 1

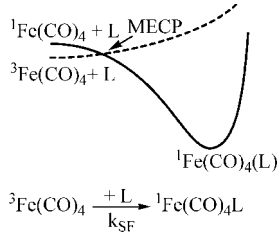

Table 1. Relative Potential Energies (kcal mol^{-1}) of Different Species at the B3PW91**/TZV Level (Values in Parentheses Include a Correction for ZPE)

	L = CO	$L = H_2$	L = Xe
$^3Fe(CO)_4 + L$	0.0 (0.0)	0.0 (0.0)	0.0 (0.0)
$^1Fe(CO)_4 + L$	3.5 (4.2)	3.5 (4.2)	3.5 (4.2)
MECP_$^{1,3}Fe(CO)_4$	6.9 (6.3)	6.9 (6.3)	6.9 (6.3)
$Fe(CO)_4$_L MECP	−1.0 (−1.3)	6.4 (6.3)	6.7 (6.1)
$Fe(CO)_4L$	−44.7 (−41.2)	−21.1 (−16.3)[a]	−2.6 (−1.2)

[a] Values for $Fe(CO)_4(H_2)$.

The calculated bond energies are in reasonable agreement with experiment and with previous CCSD(T) calculations.[34]

We initially considered the addition of ligand to $Fe(CO)_4$ to occur as shown in Scheme 1, through an MECP between the triplet and singlet surfaces, which arises due to the fact that the triplet surface is almost entirely repulsive in all cases, whereas the singlet surface is uniformly attractive. Energies for the corresponding MECPs are included in Table 1, and the geometries are shown schematically in Figure 5. In each case, the structure is such that the incoming ligand (CO, H_2, or Xe) is approaching the iron atom within the equatorial plane of the truncated trigonal bipyramid, with a distance considerably larger than that in the final adduct (r(Fe−C) = 2.220 and 1.795 Å, respectively, for MECP_CO and $Fe(CO)_5$, r(Fe−H) = 2.384 and 3.313 Å for MECP_H_2 versus 1.586 Å for $Fe(CO)_4(H_2)$ and 1.514 Å for $Fe(CO)_4(H)_2$, and r(Fe−Xe) = 3.454 and 2.773 Å, respectively, for MECP_Xe and $Fe(CO)_4Xe$). As noted previously,[7,15] the optimum geometry for the MECPs involves approach of the ligands away from the 2-fold axis of symmetry of $Fe(CO)_4$.

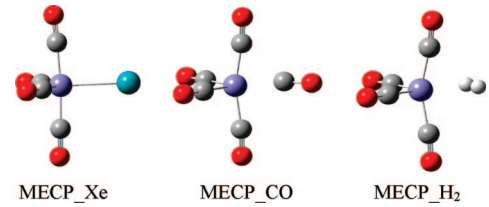

Figure 5. Geometries for the MECPs for addition of Xe, CO, and H_2 to $^3Fe(CO)_4$.

Contrary to what one might expect from the qualitative one-dimensional potential energy surfaces in Scheme 1, the MECPs for addition of Xe and H_2 lie *higher* in energy than the separated ligand and singlet $Fe(CO)_4$. This is explained by the fact that the true potential energy surfaces are highly multidimensional. Triplet and singlet $Fe(CO)_4$ have somewhat different geometries, and reaching an MECP requires significant changes in bond lengths and angles with respect to both minima. The importance of these deformations can be illustrated by the fact that the *vertical* excitation energy of triplet $Fe(CO)_4$, i.e., the energy difference between the triplet and the singlet at the optimized geometry of the triplet, is 20.7 kcal/mol (without including ZPE) at the B3PW91** level, much higher than the adiabatic excitation energy 4.2 kcal·mol^{-1}. The MECP represents the lowest energy crossing point in the multidimensional space. The fact that it lies higher in energy than the singlet fragments is consistent with the fact that the singlet surface is uniformly attractive.

Geometries and energies for the MECPs for addition of CO and H_2 have been reported previously[7,15] using slightly different levels of theory to those used here, and the present results are fairly similar to the previous ones. In particular, although the B3PW91** level of theory predicts a much smaller triplet−singlet gap for $Fe(CO)_4$ (4.2 vs 6.9 kcal/mol) than the previously used B3PW91*, the decrease in the relative energy of the MECP for the addition of H_2 is much smaller (7.7 kcal/mol with B3PW91* and 6.4 kcal/mol with B3PW91**). The previously reported MECP for CO addition was very slightly above the separated reactants (0.5 kcal/mol at the B3PW91* level). The present MECP lies slightly *below* the reactants, at −1.0 kcal/mol. This negative energy is due to the existence of a weakly bound triplet adduct. The latter species also lies at −1.0 kcal/mol (without correction for ZPE, −0.3 kcal/mol with ZPE) and is very similar in geometry to triplet $Fe(CO)_4$, with an additional weakly interacting CO ligand (r(Fe−C) = 2.221 Å).

Using the previously described[3,7] form of nonadiabatic transition state theory, it is possible to calculate bimolecular rate coefficients for this direct addition process. This requires, as well as the geometry and relative energy of the MECP, properties such as the rotational constants and vibrational frequencies of the reactants and the MECP, the slope of the potential energy surfaces at the MECP, and the magnitude of the root-mean-square spin−orbit coupling matrix element H_{soc} between the singlet and triplet electronic states at the MECP. Most of these properties are obtained directly from the previously mentioned geometry optimizations, frequency calculations, and MECP optimizations. The vibrational frequencies were computed using the effective Hessian method previously described,[8] and the H_{soc} value calculated previously[7] for the $Fe(CO)_4$ + CO system was used for all three reactions. As the H_{soc} value is a one-electron property mainly associated with the iron-based orbitals containing unpaired electrons, it is not expected to be highly sensitive either to the level of theory or the nature of the incoming ligand. We assume that the rate coefficients for reaction in the supercritical media can be modeled using gas phase transition state

Table 2. Calculated and Experimental Rate Constants for Addition of CO, H_2, and Xe to $^3Fe(CO)_4$ in cm^3 $molecule^{-1}$ s^{-1} and Calculated Activation Energies in kcal mol^{-1}

	CO	H_2	Xe
k_{sf}[a]	7.04×10^{-14}	1.71×10^{-17}	6.85×10^{-17}
E_a	−0.6	6.3	6.8
k_{exp}	5.2×10^{-14}[b]	2.0×10^{-14}[c]	*ca.* 10^{-14}[d]

[a] k_{sf} calculated at 300 K; [b] References 16, 17, and 22; experimental conditions: 0.1−1.1 psi CO (0.2−10.6 psi total pressure), 295 K. [c] Reference 41; experimental conditions: 1−9.7 psi H_2 (10.6 psi total), 296.5 K. [d] Reference 28; experimental conditions: supercritical fluid measurement, 450 psi of Xe (in *sc*Ar 4500 psi).

theory, which is reasonable for reactions involving weakly polar species in nonpolar solvents.[55]

The resulting calculated bimolecular rate constants, k_{sf}, are shown in Table 2. As can be seen, the agreement with experiment in the case of the addition of CO is good, with k_{sf} roughly 1.5 times larger than the experimental rate constant. The previously reported calculated value for k_{sf}, 8.8×10^{-15} cm^3 $molecule^{-1}$ s^{-1}, was in slightly less good agreement with the experimental value. The difference between the two calculated values is due to the different geometry and energy of the MECP in the two studies. In our previous work, we noted that two effects accounted for the fact that k_{sf} was ca. 500 times smaller than the expected gas-phase collisional rate constant. First, the calculations showed that spin-state change occurs only once every 20 times that the system reaches the MECP, with the remaining factor of 25 accounted for by the small calculated energy barrier. Here too, we find a moderate degree of spin-forbiddenness, with an average hopping probability of $^1/_{13}$. As the present more accurate calculations predict the MECP to lie *lower* in energy than reactants, the remaining difference between the experimental and collisonal rate constants would instead be attributed to the higher vibrational entropy of the MECP bottleneck compared to the loose vibrational character of the variational transition states obtained for barrierless reactions.

The calculated rate constant for the addition of H_2 to $Fe(CO)_4$ is in much less good agreement with experiment, as it is over 1000 times smaller than the latter. Such a small value can be expected simply from the fact that the MECP lies significantly higher in energy than the reactants. This observation was already anticipated in our previous study of H_2 addition.[15] Also, the calculated activation energy (derived from an Arrhenius plot of the calculated rate constants in the range 100−400 K) is quite large, at 6.3 kcal/mol. Experiment suggests a value of 0 kcal/mol.[41] The error on this latter value is quite large due to the small range of temperatures used, but the observed variation in rate constants is not consistent with the large activation energy that we have calculated. For the addition of Xe, no bimolecular rate constant was measured under gas-phase conditions. It is possible that the low stability of the adduct would make such a measurement impossible. The first-order decay of triplet $Fe(CO)_4$ in supercritical argon containing 450 psi of Xe[28] occurs with a rate coefficient of 2×10^7 s^{-1}. Assuming a Xe number density of ca. 10^{21} molecules cm^{-3}, this corresponds to a rate constant of ca. 10^{-14} cm^3 $molecule^{-1}$ s^{-1}, again much larger than our computed values.

These discrepancies are unlikely to be due to errors in the computation of the potential energy surface or other properties of the MECP. Since our first report of the energy of the MECP for $Fe(CO)_4 + H_2$, we have used coupled-cluster theory calculations on triplet and singlet $Fe(CO)_4$ and $Fe(CO)_4(H)_2$ to calibrate the accuracy of the DFT methods we use to locate the MECP.[34] We are not able to carry out very high-level CCSD(T) calculations on the low-symmetry MECP, as this would require geometry optimization at the CCSD(T) level, which is far too expensive computationally. However, single-point CCSD(T) calculations at the geometry of the MECP optimized with the B3PW91** level of theory show that the calculated energy for the MECP that we use here is accurate.

Scheme 2

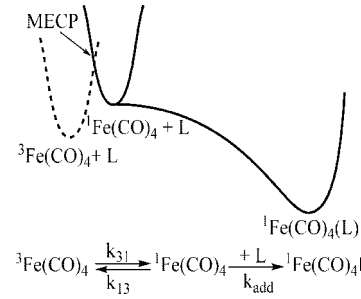

Instead, we show here that the discrepancies are due to the fact that the reaction occurs with a different mechanism from that suggested in Scheme 1, as shown in Scheme 2. In this new mechanism, triplet $Fe(CO)_4$ first converts to singlet $Fe(CO)_4$ in a unimolecular spin-forbidden step, and the singlet either reverts to the triplet through the reverse spin-forbidden step or is trapped by the ligand in a fast barrierless process to form products.

To predict rate constants for this modified mechanism, it is necessary to characterize the MECP connecting the triplet and singlet states of $Fe(CO)_4$ in the absence of an incoming ligand and to characterize the transition state for addition of ligand to singlet $Fe(CO)_4$. The MECP lies at 6.3 kcal·mol^{-1} above triplet $Fe(CO)_4$ and is thereby similar in energy to MECP_Xe and MECP_H_2. Indeed, the $Fe(CO)_4$ moiety in the latter MECPs has a similar geometry to that obtained for the MECP in the absence of ligand (Figure 6). The MECPs in the presence of the weak ligands Xe and H_2 ligands represent a very small perturbation of this "bare" MECP. The root-mean-square coupling matrix element between the triplet substates and the singlet state at this MECP is similar to that obtained previously for the $Fe(CO)_4 + CO$ MECP, at 44 cm^{-1}.

There is no barrier on the potential energy surface for the addition of CO, H_2, and Xe to $^1Fe(CO)_4$, as demonstrated by a series of partial geometry optimizations in which the metal−ligand distance is frozen. Hence the only transition state for this addition is a variational transition state due to the loss of rotational and translational entropy as the ligand adds to the metal fragment.

The rate law for the indirect addition mechanism is given by

$$v = \frac{-\mathrm{d}[^3Fe(CO)_4]}{\mathrm{d}t} = \frac{k_{31}k_{add}}{k_{13} + k_{add}[L]}[^3Fe(CO)_4][L] \qquad (1)$$

The same nonadiabatic TST code has been used to calculate k_{31} and k_{13}, as well as the equilibrium constant K_{13} between triplet and singlet iron tetracarbonyl (Table 3). Our previous high-level coupled-cluster calculations[34] suggest that the energy difference ΔE_{31} between triplet and singlet $Fe(CO)_4$ is 2.33 kcal/mol. The present B3PW91** calculations are in fair but not perfect agreement with this (calculated ΔE_{31} of 3.5 kcal/mol). If the B3PW91** energies were used directly for calculation of k_{31} and k_{31}, this would therefore lead to an incorrect equilibrium ratio k_{31}/k_{13}. We have therefore only used the B3PW91** value for the calculation of k_{31},

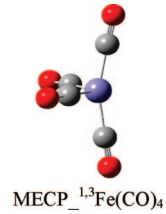

Figure 6. Geometry of the MECP $^{1,3}Fe(CO)_4$, between $^3Fe(CO)_4$ and $^1Fe(CO)_4$.

(55) Laidler, K. J. *Chemical Kinetics*, 3rd ed.; Harper and Row: New York, 1987.

Table 3. Calculated (k_{31}, k_{13}, K_{31}, k_{add} (comp), and k_{app}) and experimental (k_{exp} and k_{add} (exp)) quantities relating to addition of CO, H_2, and Xe to $^3Fe(CO)_4$ at 300 K[h]

	CO	H_2	Xe
k_{31}	$5.12 \times 10^{+6}$	$5.12 \times 10^{+6}$	$5.12 \times 10^{+6}$
k_{13}	$8.68 \times 10^{+8}$	$8.68 \times 10^{+8}$	$8.68 \times 10^{+8}$
K_{31}	5.90×10^{-3}	5.90×10^{-3}	5.90×10^{-3}
k_{add} (comp)	1.05×10^{-10}	1.31×10^{-11}	---
k_{add} (exp)	2.20×10^{-11} [b]	1.03×10^{-11} [c]	9.96×10^{-12} [d]
$k_{app} = K_{31}k_{add}$	1.30×10^{-13}	6.07×10^{-14}	5.88×10^{-14}
E_a (low pressure)	2.9	2.9	2.9
E_a (high pressure)	6.3	6.3	6.3
k_{exp} (low pressure)	5.2×10^{-14} [e]	2.0×10^{-14} [f]	
k_{exp} (high pressure)		$3.3 \times 10^{+6}$ [g]	$2.0 \times 10^{+7}$ [h]

[a] The units used are s^{-1} for k_{31}, k_{13}, and k_{exp} (high pressure), cm^3 $molecule^{-1}$ s^{-1} for k_{add}, k_{app}, and k_{exp} (low pressure) and no units for K_{31}, and kcal/mol for the energies. [b] References 11 and 22, experimental conditions: 293 K. [c] Reference 59, experimental conditions: 300 K. [d] Reference 60, 298 K. [e] Reference 16, 17, and 22, experimental conditions: 0.1−1.1 psi CO (0.2−1.1 psi total), 295 K. [f] Reference 41, experimental conditions: 1−9.7 psi H_2 (10.6 psi total), 296.5 K. [g] This work, see below. [h] Reference 28, experimental conditions: at 298 K (1500 psi Xe, 30 psi CO).

whereas, for k_{13}, the relative energy of the MECP with respect to $^1Fe(CO)_4$ was adjusted to take into account the accurate CCSD(T) energetics for ΔE_{31}. Test calculations show that the energy of the MECP relative to $^3Fe(CO)_4$ is not highly sensitive to ΔE_{31}.

The adiabatic addition rate constants k_{add} can be calculated using variational transition state theory. For different values of the metal−ligand distance, the projected vibrational frequencies are computed using the reaction path Hamiltonian[56] and combined with rotational constants to give a calculated rate constant. The latter value goes through a minimum at an intermediate value of the metal−ligand distance, and this value (shown as k_{add} (comp) for addition of CO and H_2 in Table 3) is an approximation to the true rate constant. As shown by Klippenstein et al.,[57] the use of the rigid-rotor harmonic oscillator approximation for such loose variational transition states can lead to significant overestimates of the rate constant. Also, without any calculations, this rate constant can reliably be predicted to be very close to the collisional rate constant for reaction partners of the appropriate mass. Accordingly, we have instead used in eq 1 *experimental* values of the rate constants for similar barrierless processes (see k_{add}(exp) in Table 3). The computed and experimental values are fairly similar for the addition of CO and H_2.

Given the values in Table 3, it is possible to compare our results with experimental observations. We consider first the gas phase results of Weitz et al.[16,17,22,41] These experiments use a range of ligand pressures of 5−50 (CO) and 50−500 (H_2) Torr. At the CO higher pressure, the approximate number density is 5×10^{18} molecules cm^{-3}, so that k_{add}[CO] is ca. 10^8 s^{-1} and, thereby, almost 1 order of magnitude smaller than k_{13}. For H_2, higher partial pressures are used in the experiments, but k_{add} is smaller, such that $k_{add}[H_2]$ is also significantly smaller than k_{13} over the whole experimental range. This means that eq 1 can be simplified to

$$v = \frac{k_{31}k_{add}}{k_{13} + k_{add}[L]}[^3Fe(CO)_4][L] \approx \frac{k_{31}k_{add}}{k_{13}}[^3Fe(CO)_4][L] = K_{31} \,.\, k_{add}[^3Fe(CO)_4][L] \quad (2)$$

This simplification is equivalent to stating that the second step in the mechanism, spin-allowed rapid addition of ligand to singlet iron tetracarbonyl, is rate-limiting under these conditions. The kinetics should therefore be second-order, first-order with respect to both iron tetracarbonyl and ligand, and this is indeed observed experimentally.[16,17,22,41] The apparent rate constant k_{app} is simply the product of the equilibrium constant and the spin-allowed ligand addition rate constant, as shown in Table 3. For both CO and H_2, the values obtained at 300 K are in good agreement with experiment. For H_2, this clearly shows that the indirect mechanism is the one that leads to ligand addition. Calculation of the rate constant at a small number of temperatures around 300 K (assuming k_{add} is temperature independent), followed by Arrhenius analysis, leads to a computed activation energy of 2.9 kcal/mol, which is small enough to be consistent with the observed negligible temperature dependence of the rate constant for H_2 addition. For CO addition, the direct mechanism also led to good agreement with experiment for the observed rate constant. It is therefore possible that both mechanisms contribute under these conditions, as discussed below.

We now consider the rate constants observed in supercritical fluids reported here and previously.[28] In the pure supercritical Xe (ca. 1500 psi), the number density is $\sim 8 \times 10^{21}$ molecule cm^{-3}. This gives a value of k_{add}[Xe] of 8×10^{10} s^{-1}, much *larger* than k_{13}. In other experiments,[28] 450 psi of Xe are doped into supercritical argon, corresponding to a number density of ca. 8×10^{20} molecules cm^{-3} or k_{add}[Xe] of 8×10^9 s^{-1}. In the experiment where dihydrogen is doped into supercritical argon, the typical pressure used is 90 psi. This corresponds to a number density of ca. 1.5×10^{20} molecules cm^{-3}, leading to a $k_{add}[H_2]$ value of ca. 1.5×10^9 s^{-1}, slightly larger than k_{13}. Under conditions where k_{add}[L] is larger than k_{13}, eq 1 can be simplified to

$$v = \frac{k_{31}k_{add}}{k_{13} + k_{add}[L]}[^3Fe(CO)_4][L] \approx k_{31}[^3Fe(CO)_4] \quad (3)$$

This simplification applies for trapping by pure supercritical solvent, with the experiments involving one gas doped into the supercritical fluid being at the borderline for applying this simplification. Where eq 3 applies, this corresponds to a situation in which fast trapping of $^1Fe(CO)_4$ follows slow triplet to singlet conversion. The predicted kinetics are now first order in iron tetracarbonyl only. Trapping of $^3Fe(CO)_4$ by Xe occurs with a k_{obs} of 2.0 (±0.2) × 10^7 s^{-1} in both *sc*Xe and Xe doped into *sc*Ar,[28] confirming that the rate does not depend on ligand concentration in this regime. The calculated rate constant k_{31} of 5×10^6 s^{-1} also agrees well with k_{obs} for the disappearance of $^3Fe(CO)_4$ in *sc*Xe, Xe doped in *sc*Ar (both 2.0 (±0.2) × 10^7 s^{-1}), in *sc*CH_4 (6.2 (±0.6) × 10^6 s^{-1}), and in heptane (7.6 (±0.1) × 10^7 s^{-1}). Finally, there is good agreement with the measured rate of formation of $Fe(CO)_4H_2$ from $^3Fe(CO)_4$ in *sc*Ar in the presence of H_2 (3.3 (±0.1) × 10^6 s^{-1}; see below). This suggests a common mechanism for trapping of $^3Fe(CO)_4$ in all these cases, in which triplet to singlet interconversion is rate-limiting. The slight differences in k_{obs} (ca. 1 order of magnitude from fastest to slowest) may be due to solvent effects on the relative energy of $^3Fe(CO)_4$ and the MECP, which are ignored in our calculations. Small changes in energy are plausible as solvents are known to interact significantly with $Fe(CO)_5$.[58]

Contrary to what is suggested in eq 3, trapping of $^3Fe(CO)_4$ by CO doped into supercritical argon at concentrations between 6×10^{19} and 2×10^{20} molecules cm^{-3} is however observed to follow overall second-order kinetics, first-order in both carbon monoxide and iron tetracarbonyl.[28] The measured overall rate constant 2.0×10^{-14} $molecule^{-1}$ cm^3 s^{-1} is similar to that measured in the gas

(56) Miller, W. H.; Handy, N. C.; Adams, J. E. *J. Chem. Phys.* **1980**, *72*, 99–112.
(57) Fernandez-Ramos, A.; Miller, J. A.; Klippenstein, S. J.; Truhlar, D. G. *Chem. Rev.* **2006**, *106*, 4518–4584. Klippenstein, S. J.; Georgievskii, Y.; Harding, L. B. *Phys. Chem. Chem. Phys.* **2006**, *8*, 1133–1147.
(58) (a) Lee, T.; Welch, E.; Rose-Petruck, C. G. *J. Phys. Chem. A* **2004**, *108*, 11768–11778. (b) Lessing, J.; Li, X.; Lee, T.; Rose-Petruck, C. G. *J. Phys. Chem. A* **2008**, *112*, 2282–2292.
(59) Hall, C.; Jones, W. D.; Mawby, R. J.; Osman, R.; Perutz, R. N.; Whittlesey, M. K. *J. Am. Chem. Soc.* **1992**, *114*, 7425–7435.
(60) Hunter, T. F.; Kristjansson, K. S. J. *J. Chem. Soc., Faraday Trans. 2* **1982**, *78*, 2067–2076.
(61) Kismartoni, L. C.; Weitz, E.; Cedeno, D. L. *Organometallics* **2005**, *24*, 4714–4720.

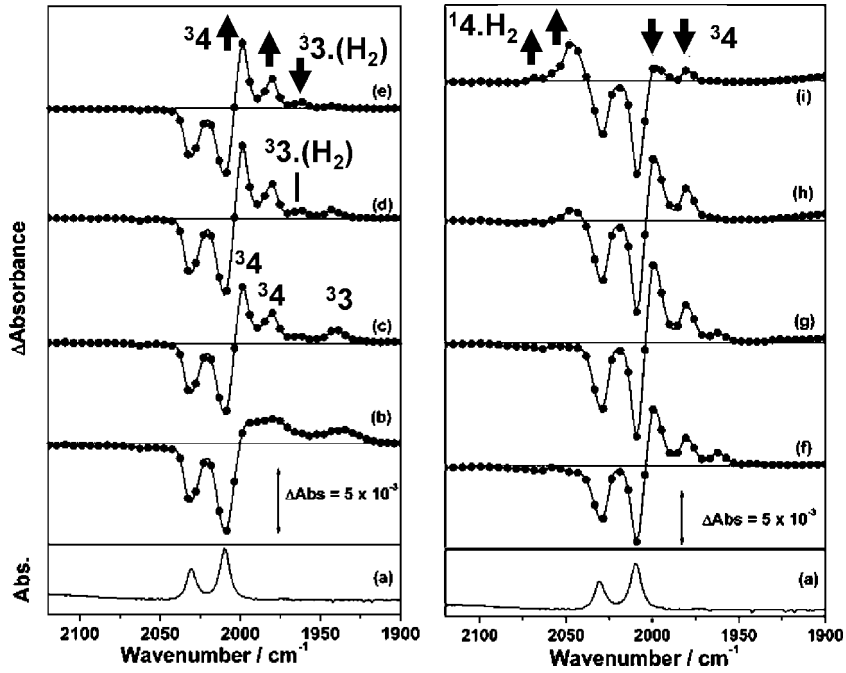

Figure 7. (a) FTIR spectrum of $Fe(CO)_5$ in scAr (4500 psi), H_2 (90 psi), and CO (60 psi) at 294 K. TRIR difference spectra of the same solution recorded at (b) 16 ps, (c) 128 ps, (d) 512 ps and (e) 1024 ps, (f) 5 ns, (g) 20 ns, (h) 100 ns, and (i) 400 ns after photolysis (267 nm). ^{3}**4** = $^3Fe(CO)_4$, ^{3}**3** = $^3Fe(CO)_3$, ^{3}**3.(H$_2$)** = $^3Fe(CO)_3(H_2)$, and ^{1}**4.H$_2$** = $^1Fe(CO)_4H_2$.

phase. At the higher concentration, k_{add}[CO] is ca. 2×10^9 s^{-1} and is thereby somewhat larger than k_{13}, but given the expected errors of at least a factor of 3 on each of these computed values, it is possible that k_{13} is in reality larger than k_{add}[CO] at these fairly low levels of CO doping, so that eq 2 applies and second-order behavior is expected. It is also possible, as discussed above, that direct addition of CO as described in Scheme 1, which is expected to follow second-order kinetics, competes with the indirect mechanism.

Spin-state change during ligand addition to a metal complex is quite a common process,[5a] so it is appropriate to comment on how general the conclusions reached here will be for other cases. This depends on the relative energy of the MECP for direct addition of ligand (as shown in Scheme 1) and that of the low-spin state of the metal fragment. If the latter species lies high in energy and the MECP is significantly lower in energy, as, e.g., for phosphine addition to $CpMoCl_2(L)$,[5b] then direct addition will predominate. If, however, the MECP lies higher in energy than the low-spin metal fragment, it is unfavorable to carry out spin change and ligand addition simultaneously, and the two-step process of Scheme 2, with initial crossover followed by spin-allowed addition, will dominate.

Photochemistry of $Fe(CO)_5$ in Solution in the Presence of Dihydrogen. The results described above demonstrate how the combination of experiment and theory can provide insights into the factors that govern spin forbidden reactions. To explore this further we have examined the photochemistry of $Fe(CO)_5$ in the presence of dihydrogen in the condensed phase.

The TRIR spectra recorded following the photolysis (267 nm) of $Fe(CO)_5$ in *sc*Ar (4500 psi), H_2 (90 psi), and CO (60 psi) at 294 K are shown in Figure 7. The TRIR spectrum recorded 16 ps after photolysis shows that the parent ν(CO) bands are bleached (2031 and 2010 cm^{-1}) and that broad transient bands to lower energy are formed. The initially formed transients are formed in vibrationally excited states. In the spectrum recorded 128 ps after photolysis, all of the transient species have cooled and individual transient bands at 1998, 1980, and 1938 cm^{-1} can be clearly identified.

The bands at 1998 and 1980 cm^{-1} are assigned to $^3Fe(CO)_4$ by comparison to the known ν(CO) frequencies of this species in *sc*Ar and in low temperature matrices.[19,28] On the picosecond time scale $^3Fe(CO)_4$ is seen to be present.

The band at 1938 cm^{-1} is assigned to $^3Fe(CO)_3$, again through comparison to previous TRIR experiments in *sc*Ar.[28] This band is seen to decay on the picosecond time scale. However the spectra recorded at the early time delays after photolysis are complicated by the presence of intermediates in a vibrationally excited state. Despite this we can estimate the observed rate constant for the decay of $^3Fe(CO)_3$ in the presence of CO (60 psi) and H_2 (90 psi) at 294 K ($k_{obs} = 1.3\ (\pm 0.5) \times 10^9$ s^{-1}). The rate of decay of $^3Fe(CO)_3$ has previously been reported in *sc*Ar with no H_2 present ($k_{obs} = 3 \times 10^9$ s^{-1}, in the presence of 30 psi of CO).[28] The similarity between the previously observed rate constant and the observed rate of decay in our experiment of $^3Fe(CO)_3$ demonstrates that no significant stabilization of this transient by H_2 occurs, supporting our assignment of the band at 1938 cm^{-1} to $^3Fe(CO)_3$.

A further weak transient band can be observed (1962 cm^{-1}) at early time delays. This band is present at an early time. On the nanosecond time scale the change in intensity of this band is found to be well fitted by a very small fast initial rise in intensity ($k_{obs} = 1.5\ (\pm 0.3) \times 10^9$ s^{-1}) and a second slower decay of this transient ($k_{obs} = 4.1\ (\pm 0.3) \times 10^7$ s^{-1}). The small fast rise of the transient at 1962 cm^{-1} matches the observed rate constant for the decay of the band at 1938 cm^{-1}, which is assigned to $^3Fe(CO)_3$, while the slower component matches the rate of a small increase in the intensity of the ν(CO) bands of $^3Fe(CO)_4$ (1998 cm^{-1}: $k_{obs} = 7.5\ (\pm 2.1) \times 10^7$ s^{-1}, 1980 cm^{-1} $k_{obs} = 5.4\ (\pm 1.8) \times 10^7$ s^{-1}).

Previous *ps*-TRIR experiments have identified initially formed transients at *ca.* 1961 cm^{-1} following the photolysis of $Fe(CO)_5$ in *sc*Ar.[28] In these studies this weak band was tentatively assigned to the initial formation of a small concentration of $^1Fe(CO)_4$ which decayed rapidly in the presence of CO ($k_{obs} = 1.4\ (\pm 0.1) \times 10^9$ s^{-1}). We initially considered if the transient observed in our study at 1962 cm^{-1} could be assigned to a small concentration of initially formed $^1Fe(CO)_4(H_2)$. This species has not been observed in gas phase TRIR studies of the reaction of $^3Fe(CO)_4$ with H_2.[41] The formation of $^1Fe(CO)_4H_2$ has been predicted to proceed *via* the formation of $^1Fe(CO)_4(H_2)$. Previous theoretical studies have suggested that the barrier to the formation of $^1Fe(CO)_4H_2$ from

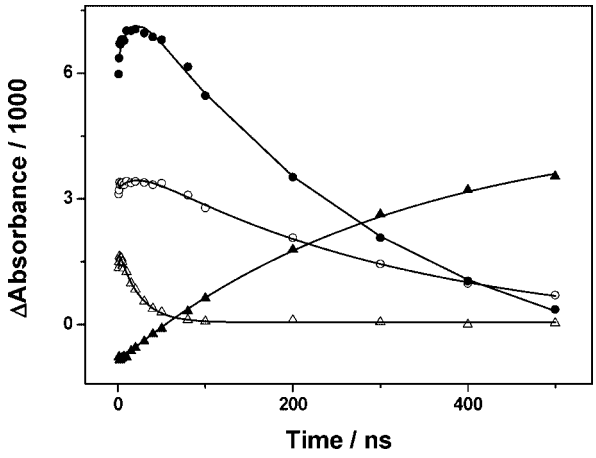

Figure 8. Kinetic traces of $^3Fe(CO)_4$ (●, 1999; ○ 1980 cm^{-1}) $^1Fe(CO)_4H_2$ (▲, 2048 cm^{-1}) and $Fe(CO)_3(H_2)$ (Δ, 1962 cm^{-1}). Recorded following the photolysis (266 nm) of $Fe(CO)_5$ in *sc*Ar (4500 psi), H_2 (90 psi), and CO (60 psi) at 294 K.

$^1Fe(CO)_4(H_2)$ is very low (<0.3 kcal mol^{-1});[15,35] therefore any initially formed $^1Fe(CO)_4(H_2)$ may be expected to rapidly react to form $^1Fe(CO)_4H_2$. In our experiments the transient at 1962 cm^{-1} has a lifetime of *ca.* 24 ns.

Gas phase TRIR experiments have identified a ν(CO) band of $^3Fe(CO)_3(H_2)$ at 1967 cm^{-1} (*cf.* $^3Fe(CO)_3$ ν(CO) at *ca.* 1950 cm^{-1} under the reported conditions),[5a] and this transient was assigned to the nonclassical dihydrogen complex, $^3Fe(CO)_3(H_2)$, based on DFT calculations. In our experiments there is evidence that the band at 1962 cm^{-1} increases slightly in intensity as the ν(CO) band of $^3Fe(CO)_3$ decays, which would support the assignment of this feature to $^3Fe(CO)_3(H_2)$. This band at 1962 cm^{-1} then decays to form $^3Fe(CO)_4$ which could correspond to the substitution of H_2 with CO in $^3Fe(CO)_3(H_2)$. The experimental data are consistent with the transient at 1962 cm^{-1} being $^3Fe(CO)_3(H_2)$, and in the following section new DFT calculations on the possible formation and reactivity of $^3Fe(CO)_3(H_2)$ are reported.

The bands of $^3Fe(CO)_4$ decay (1998 cm^{-1}: $k_{obs} = 3.3$ (±0.5) × 10^6 s^{-1}, 1980 cm^{-1} $k_{obs} = 3.2$ (±0.7) × 10^6 s^{-1}) at the same rate as a broad band (*ca.* 2045 cm^{-1}), assigned to $^1Fe(CO)_4H_2$, grows in ($k_{obs} = 3.3$ (±0.1) × 10^6 s^{-1}), Figure 8. (It may be possible to fit the rise of the ν(CO) band of $^1Fe(CO)_4H_2$ to a biexponential growth function.) However the possible fast component (*ca.* 30 ns) is very small, and it is difficult to confirm its presence. In hexane $^1Fe(CO)_4H_2$ has previously been reported to have strong ν(CO) bands at 2053 and 2042 cm^{-1} with a very weak shoulder at 2029 cm^{-1}.[43] Multi-Lorentzian fitting of the TRIR difference spectrum recorded 400 ns after photolysis indicates the broad band at 2045 cm^{-1} is made up of two ν(CO) bands centered at ~2050 and 2043 cm^{-1} and that an additional shoulder band at 2068 cm^{-1} is also present. The bleaching of the bands of $Fe(CO)_5$ around 2029 cm^{-1} means it is not possible to observe the previously reported weak shoulder band in this region. Comparison to the ν(CO) bands of $^1Fe(CO)_4H_2$ recorded in this study to a high resolution FTIR spectrum of $Fe(CO)_4H_2$ in the gas phase shows very good agreement,[41] confirming our assignment of the broadband at 2045 cm^{-1} to $^1Fe(CO)_4H_2$ (see Supporting Information). In these experiments we have not been able to identify the weak ν(M−H) stretch of $^1Fe(CO)_4H_2$ expected at *ca.* 1890 cm^{-1}. The ν(CO) bands of $^1Fe(CO)_4H_2$ are seen to be stable for the duration of this experiment (*ca.* 1 ms), and no recovery of the parent $Fe(CO)_5$ bands is observed. The proposed reaction scheme for the activation of dihydrogen following the photolysis of $Fe(CO)_5$ in *sc*Ar is shown in Scheme 3. In agreement with the gas phase TRIR experiments the key step is the reaction of $^3Fe(CO)_4$ with H_2. These experiments are, to our knowledge, the first time that the rate of activation of H_2 by $Fe(CO)_4$ has been directly monitored in a room temperature solution.

Scheme 3. Proposed Reaction Scheme for the Activation of H_2 Following the Photolysis (266 nm) of $Fe(CO)_5$ in *sc*Ar (4500 psi), H_2 (90 psi), and CO (60 psi) at 294 K

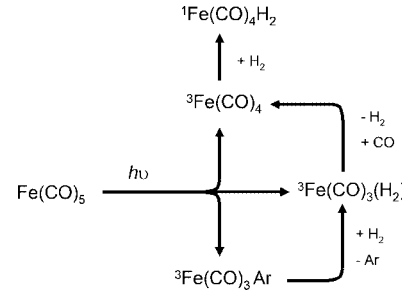

Table 4. Calculated Potential Energies (ZPE Corrected and in kcal/mol) of $Fe(CO)_3 + H_2 + CO$ Species

	ΔE		ΔE
$^3Fe(CO)_3(H_2) + CO$	0.0	$^3Fe(CO)_4 + H_2$	−25.4
$^1Fe(CO)_3(H_2) + CO$	4.8	$^1Fe(CO)_4 + H_2$	−21.3
$^3Fe(CO)_3(H)_2 + CO$	14.9	$^1Fe(CO)_4(H)_2$	−48.2
$^1Fe(CO)_3(H)_2 + CO$	−1.4	$^1Fe(CO)_4(H_2)$	−41.7
$^1TS[Fe(CO)_3(H_2) \rightarrow Fe(CO)_3(H)_2] + CO$	10.6	$^3Fe(CO)_3 + H_2 + CO$	9.8
MECPa $Fe(CO)_3(H_2) + CO$	6.6	$^1Fe(CO)_3 + H_2 + CO$	24.0
MECPb ($Fe(CO)_3(H_2)$—CO)	6.1		
$TS[^3Fe(CO)_3(H_2) + CO \rightarrow {}^3Fe(CO)_4 + H_2]$	−0.2		

We have also explored the chemistry of photoproducts of $Fe(CO)_5$ in supercritical argon doped with H_2 using computation, with a focus on confirming the identification of the minor species formed on the picosecond time scale as $^3Fe(CO)_3(H_2)$, and accounting for the observed rate of its decay ($k_{obs} = 4.1$ (±0.3) × 10^7 s^{-1}). Our calculations show that both singlet and triplet $Fe(CO)_3(H_2)$ dihydrogen complexes are bound with respect to $^3Fe(CO)_3 + H_2$, the likely precursor of the observed species (Table 4). Triplet $Fe(CO)_3(H_2)$ is more stable than the singlet by 4.8 kcal/mol. We have also located dihydride species $^{1,3}Fe(CO)_3H_2$. The triplet form is much less stable than the dihydrogen complexes and, hence, can be disregarded, but the singlet lies 1.4 kcal/mol lower in energy than $^3Fe(CO)_3(H_2)$. However, this species is unlikely to be formed, as the TS for insertion into the dihydrogen bond lies high in energy.

If formed, the singlet dihydrogen complex $Fe(CO)_3(H_2)$ would be expected to decay extremely rapidly, as we have found that it can add carbon monoxide to yield $Fe(CO)_4(H_2)$ without a barrier on the potential energy surface. Such a barrierless reaction would have a rate constant of ca. 10^{-11} cm^3 $molecule^{-1}$ s^{-1}, which would yield a pseudo-first-order rate constant of ca. 10^9 s^{-1}, which does not agree with the observed experimental rate. Furthermore the addition of H_2 to $^3Fe(CO)_3$ or to the weakly bound $^3Fe(CO)_3Ar$ would be expected to proceed in a spin-allowed way, to form the more stable $^3Fe(CO)_3(H_2)$ rather than the singlet.

The most likely assignment for the observed intermediate is therefore $^3Fe(CO)_3(H_2)$ as discussed above. We explored whether the likely decay of this species is consistent with its observed lifetime. Three possible mechanisms were considered. First, a spin-state change of $^3Fe(CO)_3(H_2)$ to $^1Fe(CO)_3(H_2)$ or $^1Fe(CO)_3H_2$ could occur, followed by rapid addition of CO. There is no MECP leading directly to the more stable dihydride species, and the MECP connecting to the singlet dihydrogen complex (MECPa) lies at 6.6 kcal/mol. This would be expected to lead to a rate constant for a triplet-singlet spin state change on the order of 10^6 s^{-1}, as above for $Fe(CO)_4$. A second possibility is direct spin-forbidden addition of CO. The triplet $Fe(CO)_3(H_2) + CO$ surface is repulsive, so the MECP with the singlet surface (MECPb) lies higher in energy, at 6.1 kcal/mol. Based on our results for the reactions of $^3Fe(CO)_4$, this high energy excludes a rapid reaction through this MECP.

Finally, we considered a spin-allowed substitution reaction between CO and $^3Fe(CO)_3(H_2)$ to give $^3Fe(CO)_4$ and H_2. A concerted TS for this process was located, lying 0.2 kcal/mol lower in energy than separated $^3Fe(CO)_3(H_2)$ and CO at the B3PW91**/TZP level of theory. The presence of a low barrier on the energy surface for this substitution is consistent with a bimolecular rate constant at 300 K slightly lower than the collisional limit, on the order of 10^{-12} cm^3 s^{-1}, corresponding, with a CO number density of 1.06×10^{20} molecules cm^{-3}, to a predicted decay rate of ca. 10^8 s^{-1}, in reasonable agreement with the observed rate, $k_{obs} = 4.1$ ($\pm$0.3) $\times$ 10^7 s^{-1}. Hence we suggest that the most plausible interpretation of the experimental decay process is that it corresponds to a spin-allowed substitution of H_2 by CO in $^3Fe(CO)_3(H_2)$.

Conclusions

New experimental results are provided for the reactivity of $Fe(CO)_4$ and $Fe(CO)_3$ produced upon photolysis of iron pentacarbonyl in liquid heptane and in supercritical rare gases. The rate of addition of CO, heptane, Xe, and H_2 to $Fe(CO)_4$ is measured under a number of different conditions, using the PIRATE setup and ultrafast flash photolysis/infrared spectroscopy methods. Careful studies of the temperature dependence of the rate constants were carried out, showing that solvent addition in *sc*Xe and heptane involves a significant activation barrier of 7.1 ($\pm$0.5) and 5.2 ($\pm$0.2) kcal mol^{-1}, respectively. Photolysis of iron pentacarbonyl in *sc*Ar doped with H_2 is shown to lead to a number of species, including a small amount of a species assigned as $^3Fe(CO)_3(H_2)$ that decays rapidly with a k_{obs} of 4.1 ($\pm$0.3) $\times$ 10^7 s^{-1}. Computational work provides support for the assignment of this transient species as a triplet dihydrogen complex and also accounts for the observed rate of loss of this species upon reaction with CO.

Extensive new computational work is also presented to account for the kinetics of ligand addition to $^3Fe(CO)_4$, based on accurate DFT calculation of singlet and triplet potential energy surfaces and of their intersections. Many of these reactions are spin-forbidden and hence are very challenging targets for the prediction of rate constants. Although results of theoretical investigations on some of these reactions had been reported previously, the present results account for a much wider range of observations, including results from new experiments given here, some of which were suggested by the computational work.

The DFT calculations use a modified form of B3PW91 with a reduced amount (10%) of exact exchange, which has been chosen as it yields calculated energies for a number of species, especially triplet and singlet iron tetracarbonyl, that agree well with high-level calibration results at the CCSD(T) level. For addition of CO to $^3Fe(CO)_4$, good agreement with the experimental second-order rate constant is obtained in nonadiabatic transition state theory calculations that assume a "direct" mechanism, in which ligand addition and spin-state change occur in a single, bimolecular, step.

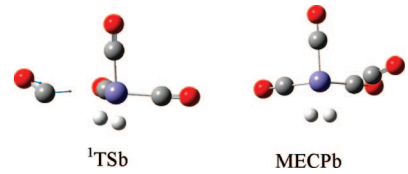

Figure 9. Optimized geometries for the concerted transition state (^{3}TSc), between $^3Fe(CO)_3(H_2)$ + CO → $^3Fe(CO)_4$ + H_2 and the MECPb {$^3Fe(CO)_3(H_2)$ + CO → $^1Fe(CO)_4(H_2)$}.

Very poor agreement with experiment is however obtained for addition of H_2 or Xe when assuming a similar direct mechanism. Instead, an indirect mechanism involving initial spin crossover of $^3Fe(CO)_4$ to $^1Fe(CO)_4$ followed by barrierless addition of ligand on the singlet potential energy surface is proposed. This mechanism was initially considered to be implausible for a number of reasons, including the experimental observation of second-order kinetics for gas phase addition of H_2[41] and the low measured temperature dependence of the measured rate constant.[41] Most previous computational work predicted that the singlet state of $^1Fe(CO)_4$ was significantly higher in energy than the triplet, so that a stepwise mechanism of the type proposed here would have led to a large observed activation energy. Accurate calculations however show a relatively small spin-state splitting,[34] which means that the stepwise mechanism is consistent with the observed low activation energy for reaction with H_2. Indeed, calculation of the individual rate constants for the elementary steps in the indirect addition mechanism, combined with the concentrations used in the gas phase and solution experiments, leads to very good agreement between observed and calculated rates and also accounts for the observed order of reaction under the different conditions.

Acknowledgment. We thank the EPSRC and EU (PP) for funding. J.N.H. thanks the EPSRC for an Advanced Research Fellowship and Rinaldo Poli for helpful discussion at an early stage of this project. M.W.G. gratefully acknowledges receipt of a Royal Society Wolfson Merit Award. We thank STFC for facility access to the Laser for Science Facility at the Rutherford Appleton Laboratory and Professors A. W. Parker and P. Matousek for useful discussions.

Supporting Information Available: Complete ref 47; calculation and experimental details. This material is available free of charge via the Internet at http://pubs.acs.org.

JA807149T